

Sensor and Simulation Notes

Note 410

September 1997

**Design of a Feed-Point Lens with Offset Inner Conductor  
for a Half Reflector IRA with  $F/D$  Greater than 0.25**

W. Scott Bigelow

Everett G. Farr

*Farr Research, Inc.*

**Abstract**

An important component of a high-voltage half reflector impulse radiating antenna (HIRA) is the feed-point lens. Designs are available to feed reflectors which have focal length to diameter ratios ( $F/D$ ) equal to 0.25, but the theory for higher  $F/D$  ratios has not been available. We develop here the theory for  $F/D$  ratios larger than 0.25. We retain a rotationally symmetric lens; but the lens is now penetrated by an off-axis inner conductor. This conductor is offset such that the charge center follows a ray path, from the input feed, through the lens, which emerges at the specific angle required to obtain the target  $F/D$  ratio.

## 1. Introduction

Design equations were developed in [1] for the dielectric feed-point lens used to match an electrically large coaxial waveguide to the feed arms of a high-voltage half reflector impulse radiating antenna (HIRA). This lens converts a plane wave in the coaxial waveguide to a spherical wave launched onto the conical feed arms of the antenna. In [2], the design equations were refined by incorporation of an impedance matching condition between the input and output of the lens. Since the problem could be solved semi-analytically only for a rotationally symmetric geometry, a single conical feed and a  $0.25 F/D$  (parabolic reflector focal length to diameter) ratio were assumed. Here we extend that design approach to obtain an approximate solution for HIRAs with feeds that break the rotational symmetry. This permits consideration of HIRAs with  $F/D$  ratios larger than 0.25. As an example, we examine a high-voltage HIRA with an  $F/D$  ratio of 0.40. Potential advantages of a larger  $F/D$  ratio are reduced pre-pulse to impulse ratio in the radiated field, and improved low-frequency performance.

In extending the design approach for HIRAs with rotationally symmetric feeds to those with  $F/D$  greater than 0.25, the lens design remains rotationally symmetric; but the lens is penetrated by an off-axis inner feed conductor. Thus, in the region behind the lens, the charge center

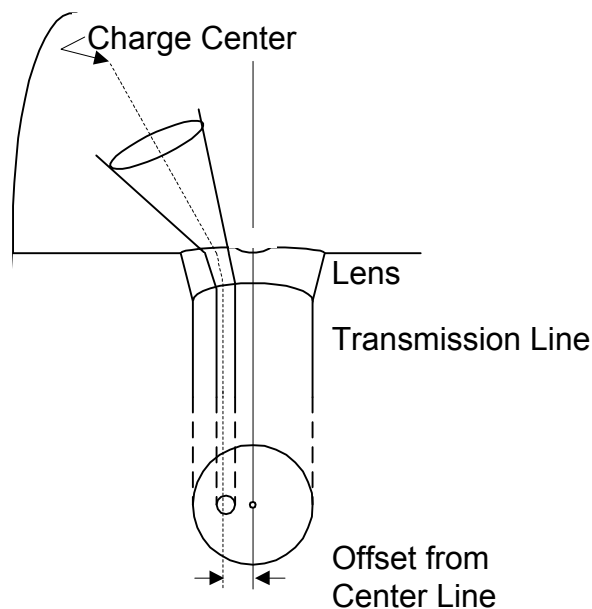


Figure 1. Concept for a HIRA with offset inner conductor and rotationally symmetric feed-point lens.

is parallel to, but no longer coaxial with the outer conductor. Within and beyond the lens, the inner conductor is bent and flared to match the ray paths in those regions. Thus, at the output of the lens, the geometry is that of a bent cone over a ground plane. The concept is illustrated here in Figure 1.

The  $F/D$  ratio of the reflector determines the angle that the charge center of the output cone must make with the ground plane—the bend angle of the charge center of the cone [3 (14)]. This angle, in conjunction with the desired output impedance, determines the angle between the axis of the output cone and the ground plane—the bend angle of the cone axis [3 (15)]. In turn, the half angle of the

output cone is determined by the bend angle and by the desired feed impedance [3 (16)]. The equations governing the cone angles referenced here are introduced in the derivation that follows.

Conformal mapping between the input transmission line and the aperture plane provides a relationship between the  $F/D$  ratio and the relative radial offset of the charge center from the axis of the input transmission line [2 (A.2.7)]. Thus, both the bend angle and the relative offset are established by the reflector  $F/D$  ratio. Impedance matching to the bent cone output determines the relative conductor radii in the transmission line, and the peak electric field on the inner conductor places lower limits on conductor dimensions [4 (4.1) and (4.5)].

By retaining the rotational symmetry of the lens, we implicitly assume that the rays emerge from the quartic lens surface in a spherical wavefront. The inner conductor is offset such that the charge center follows the ray path from the input transmission line through the lens, which emerges at the specific angle required to obtain the target  $F/D$  ratio. The rays associated with the inner conductor axis and surface also follow paths determined by the lens design. Although the charge center ray exits the lens at the correct angle, we find that the other rays exit the lens at angles slightly different from the intended ones.

In the material that follows, we derive the relationships between the  $F/D$  ratio of the reflector and the input transmission line geometry; and we show how the rotationally symmetric lens is integrated into the offset feed design. We also present a HIRA design calculation for an  $F/D$  ratio of 0.40, in which the transmission line and reflector feed are designed to an impedance of  $100 \Omega$  in air.



given by a similarly modified version of [3 (16)]

$$\alpha = \arcsin\left(\frac{\sin(\beta)}{\cosh(2\pi f_g)}\right) \quad (2.3)$$

where the characteristic impedance is  $Z_C = f_g Z_0$ , and  $Z_0 = 376.727 \Omega$ . Thus,  $f_d = F/D$ , alone determines  $\beta_0$ . The other two cone angles,  $\alpha$  and  $\beta$ , are determined by both  $f_d$  and  $f_g$ .

The next step in the derivation is to relate the reflector focal length to aperture diameter ratio,  $f_d = F/D$ , to the radial offset of the charge center in the input feed line. We use a result of the conformal mapping presented in [2 (A.2.7)], which relates  $y$  (height) in the aperture plane to  $\Psi$  (radial position) in the input feed,

$$\frac{y}{d_a} = \frac{1 - \Psi / \Psi_1}{1 + \Psi / \Psi_1} \quad (2.4)$$

where  $d_a$  is the radius of a parabolic dish with focus in the plane of the dish edge, the case for which  $f_d = 0.25$ ; and  $\Psi_1$  is the radius of the outer conductor of the input feed line. This relationship is valid in the  $z = 0$  plane for  $y$  on a line between  $(x_0, 0, 0)$  and  $(x_0, y_0, 0)$ , and for  $\Psi = -x$  on the closed interval  $-\Psi_1 \leq x \leq 0$ . Here,  $y_0$  is the intersection, corresponding to the  $F/D$  ratio of interest, of the charge center with the parabola. Within the cylindrical transmission line, we let  $\Psi_{CC1}$  be the corresponding offset of the charge center from the axis of the outer conductor. Then, upon rearranging, (2.4) becomes

$$\frac{\Psi_{CC1}}{\Psi_1} = \frac{1 - y_0 / d_a}{1 + y_0 / d_a} \quad (2.5)$$

Since  $y_0 = D / 2$  and  $d_a = 2F$ , we have  $y_0 / d_a = 1/(4f_d)$ . Thus (2.5) becomes

$$\frac{\Psi_{CC1}}{\Psi_1} = \frac{1 - 1/(4f_d)}{1 + 1/(4f_d)} \quad (2.6)$$

Like the charge center exit angle,  $\beta_0$ , we see that this ratio depends only on the assumed  $F/D$  ratio.

Now that we have the ratio of the offset of the charge center to the transmission line radius,  $\Psi_{CC1} / \Psi_1$ , we derive the remainder of the transmission line parameters.

## 2.2 Derivation of the Characteristic Parameters of the Offset Transmission Line

For a cylindrical transmission line feed with offset inner conductor, we have from [5 (6)], the conformal transformation

$$\frac{\zeta}{d} = j \coth(w/2) \quad (2.7)$$

where  $w = u + jv$  and  $\zeta = x + jy$ . This leads to the following complex map (Figure 3 on page 7), where circles of constant  $u$  (equipotentials) and lines of constant  $v$  (electric field lines) are mutually orthogonal. Since dimensions in the complex map are normalized, the axes are in dimensionless units of  $x/d$  and  $y/d$ , where  $d$  is the distance from the charge center to a virtual ground plane. The surfaces of the inner and outer conductors are indicated in the figure at the  $u$ -contours,  $u = u_0$ , and  $u = u_1$ , respectively. Below, we show that these contours are determined by our choices of  $f_d$  and  $Z_C$ .

We continue our derivation with reference to the complex map introduced in Figure 3. If we let  $\Psi_0$  be the radius of the inner transmission line conductor, and if we let  $\Psi_{CC0}$  be the offset of the charge center from the axis of the inner conductor, then, from [6 (3.1)] or [5 (17)], we have

$$(d + \Psi_{CC1})^2 = d^2 + \Psi_1^2 \quad (2.8)$$

and

$$(d + \Psi_{CC0})^2 = d^2 + \Psi_0^2 \quad (2.9)$$

We solve (2.8) for the ratio,  $d / \Psi_1$ , obtaining

$$\frac{d}{\Psi_1} = \frac{1}{2} \left[ \frac{\Psi_1}{\Psi_{CC1}} - \frac{\Psi_{CC1}}{\Psi_1} \right] \quad (2.10)$$

From [6 (3.5)] we have for the normalized ordinate

$$\frac{y}{d} = \frac{\sinh u}{\cosh u - \cos v} \quad (2.11)$$

Now, at the top of the  $u = u_1$  circle,  $v = 0$ ; and at the bottom,  $v = \pi$ . Thus

$$\frac{y_{1,\text{top}}}{d} = \frac{\sinh u_1}{\cosh u_1 - 1} \quad \text{and} \quad \frac{y_{1,\text{bottom}}}{d} = \frac{\sinh u_1}{\cosh u_1 + 1} \quad (2.12)$$

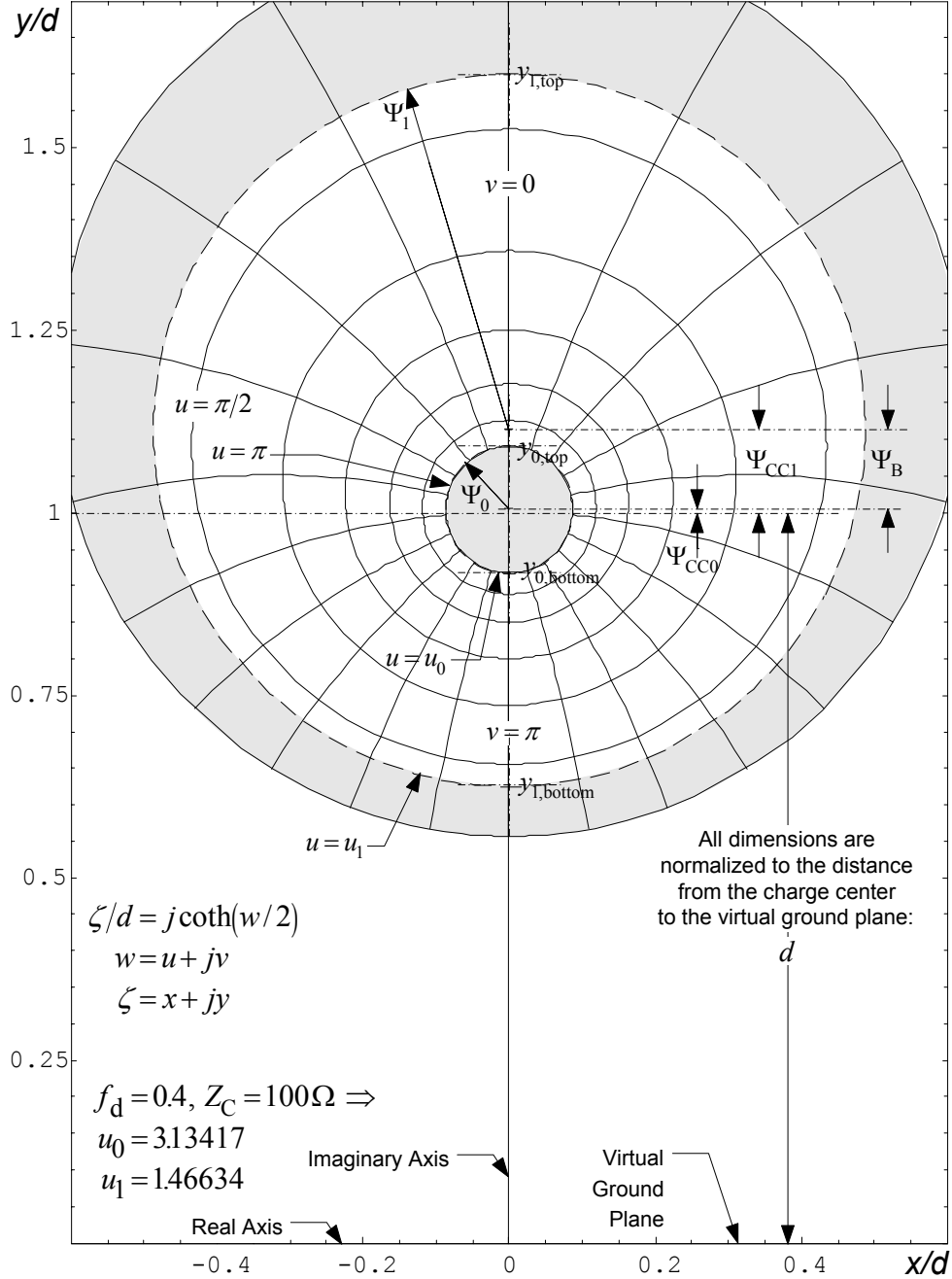


Figure 3. Complex potential map of a cylindrical feed line with offset inner conductor. The axes of the outer and inner conductors are separated by the distance,  $\Psi_B$ . On this map, all dimensions are normalized to the distance,  $d$ , from the charge center to the virtual ground plane. The equipotentials,  $u_0$  and  $u_1$  are determined by the  $F/D$  ratio and by the impedance,  $Z_C$ .

and

$$\frac{y_{1, \text{top}} - y_{1, \text{bottom}}}{d} = \frac{2\Psi_1}{d} = \frac{\sinh u_1}{\cosh u_1 - 1} - \frac{\sinh u_1}{\cosh u_1 + 1} \quad (2.13)$$

This can be simplified to obtain

$$\frac{d}{\Psi_1} = \sinh u_1 \quad (2.14)$$

from which we readily obtain  $u_1$ . Since  $f_g = \Delta u / \Delta v = (u_0 - u_1) / 2\pi$ , we obtain  $u_0$  from

$$u_0 = u_1 + 2\pi f_g \quad (2.15)$$

In a manner analogous to that used to obtain (2.14), we have

$$\frac{d}{\Psi_0} = \sinh u_0 \quad (2.16)$$

Since we know  $d / \Psi_1$  from (2.10), we now have the ratio of the transmission line conductor radii

$$\frac{\Psi_0}{\Psi_1} = \frac{d/\Psi_1}{d/\Psi_0} \quad (2.17)$$

To obtain an expression for  $\Psi_{CC0} / \Psi_1$ , we divide (2.9) by  $\Psi_1^2$ , take the square root, and solve for  $\Psi_{CC0} / \Psi_1$

$$\Psi_{CC0} / \Psi_1 = \sqrt{(d/\Psi_1)^2 + (\Psi_0/\Psi_1)^2} - d/\Psi_1 \quad (2.18)$$

Since the axis of the inner conductor is at  $(x, y) = (0, d + \Psi_{CC0})$  in the complex plane, and the axis of the outer conductor is at  $(x, y) = (0, d + \Psi_{CC1})$ , the offset or separation of the inner conductor axis from the outer conductor axis is obtained from

$$\Psi_B / \Psi_1 = \Psi_{CC1} / \Psi_1 - \Psi_{CC0} / \Psi_1 \quad (2.19)$$

where  $\Psi_{CC1} / \Psi_1$  is calculated by (2.6), and  $\Psi_{CC0} / \Psi_1$  is obtained from (2.18). Since the radial position of the outer conductor axis is taken to be  $\Psi = 0$ , we have that  $\Psi_B$  is also the radial coordinate of the axis of the offset inner conductor.

The offset transmission line feed is completely specified in terms of three physical parameters,  $\Psi_1$ , the outer conductor radius,  $\Psi_0$ , the inner conductor radius, and  $\Psi_B$ , the radial

offset of the axis of the inner conductor. At this point, we know how both of the other parameters scale with  $\Psi_1$ .

### 2.3 Using the Peak Electric Field to Set Minimum Feed Line Dimensions

To complete the specification of the offset transmission line parameters, we need only specify the radius of either conductor. In doing so, we want to keep the peak electric field in the line below some maximum, as in [1 (5.2)] for the rotationally symmetric case. The peak field in the offset feed line occurs on the surface of the inner conductor, on the side nearest the outer conductor. In the complex plane, this occurs at  $(x, y) = (0, d + \Psi_{CC0} - \Psi_0)$ . At this point, the  $x$ -component of the electric field vanishes by symmetry; and, from [7 (4.4)], we have

$$E_y(x=0, y) = \frac{-V_0}{\Delta u} \left. \frac{\partial u(x=0, y)}{\partial y} \right|_{y=d+\Psi_{CC0}-\Psi_0} \quad (2.20)$$

where  $V_0$  is the electrical potential on the inner conductor and from [7 (4.5)]

$$u(x=0, y) = \ln \left( \frac{1+y/d}{1-y/d} \right) \quad (2.21)$$

Thus, the derivative in (2.20) is just  $\partial u(x=0, y)/\partial y = 1/(d+y) + 1/(d-y)$ . At the hot spot

$$\left. \frac{\partial u(x=0, y)}{\partial y} \right|_{y=d+\Psi_{CC0}-\Psi_0} = \frac{1}{2d - (\Psi_0 - \Psi_{CC0})} + \frac{1}{\Psi_0 - \Psi_{CC0}} \quad (2.22)$$

By using  $\Delta u = 2\pi f_g$  and the result of (2.22) in (2.20), we obtain after some rearranging

$$\Psi_{1,\min} = \frac{V_0}{2\pi f_g E_{\max}} \left[ \frac{1}{\Psi_0/\Psi_1 - \Psi_{CC0}/\Psi_1} - \frac{1}{\Psi_0/\Psi_1 - \Psi_{CC0}/\Psi_1 + \Psi_{CC1}/\Psi_1 - \Psi_1/\Psi_{CC1}} \right] \quad (2.23)$$

where  $E_{\max} = E_y$  is the maximum field permissible at the hot spot, and  $\Psi_{1,\min}$  is the minimum permissible outer conductor radius for the stated values of  $E_{\max}$  and  $V_0$ . Any larger radius can be chosen.

With  $\Psi_1$  known,  $\Psi_0$  is obtained from (2.17); and  $\Psi_B$  is obtained from (2.19). We turn now to design of a rotationally symmetric feed-point lens to integrate with the offset feed.



where  $K_Z = \exp(2\pi f_{g, \text{monocone}}) = \exp(2\pi Z_{C, \text{monocone}}/Z_0)$ . Since, here we use  $\mathcal{G}_0 = 90^\circ - \beta_0$ , we simply calculate the constant,  $K_Z$ , by inversion of (3.1), rather than basing it on impedance.

From this point, the lens design algorithm proceeds exactly as for the rotationally symmetric,  $F/D = 0.25$ , HIRA. We summarize that method here. Later, we present a sample design calculation using this approach.

### 3.2 Lens Design Algorithm as Applied to a HIRA with Offset Feed

As described above, there are only minor adjustments required to adapt the lens design approach described in [2] to the case of a rotationally symmetric lens used with an offset feed. Three parameters normally established at the start of the design calculation are now determined by a prior offset feed design calculation: (1) the exit ray monocone half angle,  $\mathcal{G}_0$ , is determined by  $\beta_0$ , the angle between the emerging charge center and the ground plane; (2) the inner conductor radius,  $\Psi_{0, \text{lens}}$ , is taken to be the radial coordinate of the offset charge center,  $\Psi_{CC1}$ ; and (3) the outer conductor radius for the offset feed,  $\Psi_1$ , is also the outer conductor radius for the lens design. A fourth parameter, the lens radius at the ground plane,  $\Psi_2$ , remains arbitrary, subject to the minimum required to ensure that the lens has non-zero thickness on axis, and that electrical breakdown does not occur between the emerging offset feed and the ground plane.

We begin the design algorithm by numerically solving [2 (2.17)] for the conductor flare angles,  $\theta_1$  and  $\theta_0$ , as shown above in Figure 4,

$$\frac{-\csc \mathcal{G}_0 + \sqrt{\varepsilon_{r2}} \left( \cot \mathcal{G}_0 - x_0 + \sqrt{1+x_0^2} \right)}{-\csc \mathcal{G}_0 + \cot \mathcal{G}_0 - x_0 + \sqrt{\varepsilon_{r2}} \sqrt{1+x_0^2}} = \frac{-1 + \sqrt{\varepsilon_{r2}} \left( -x_1 + \sqrt{1+x_1^2} \right)}{-1 - x_1 + \sqrt{\varepsilon_{r2}} \sqrt{1+x_1^2}} \quad (3.2)$$

where we have made the change of variable,  $x_i = \cot \theta_i$ ; and where, from [2 (2.18)], we have

$$x_0 = - \frac{K_Z \left( \left( 2x_1 - 2\sqrt{\varepsilon_{r1}} \sqrt{1+x_1^2} \right) - \left( 2x_1 - 2\sqrt{\varepsilon_{r1}} \sqrt{1+x_1^2} \right) \right)}{2(-1 + \varepsilon_{r1})} - 2 \left( \varepsilon_{r1} - K_Z^2 \left( \varepsilon_{r1} - x_1^2 (1 + \varepsilon_{r1}) + 2x_1 \sqrt{\varepsilon_{r1}} \sqrt{1+x_1^2} \right) \right) \quad (3.3)$$

and  $K_Z = \cot(\mathcal{G}_0/2)$ ,  $\varepsilon_{r1} = \varepsilon_2/\varepsilon_1$ , and  $\varepsilon_{r2} = \varepsilon_2/\varepsilon_3$ . After using (3.3) to eliminate  $x_0$  from (3.2), we use Newton's method to solve for  $x_1 = \cot \theta_1$ . Next,  $x_0$  is obtained from (3.3); and  $\theta_1$  and  $\theta_0$  are recovered as  $\text{arccot}(x_1)$  and  $\text{arccot}(x_0)$ , respectively.

This completes the lens design, save specification of the output lens radius,  $\Psi_2$ . The parameters of the ellipsoidal surface,  $a$  and  $d$ , are obtained from [2 (2.11)] and [1 (3.2)] as

$$a = \frac{\sqrt{\varepsilon_{r1}}}{\varepsilon_{r1}-1} (\cot \theta_1 + \sqrt{\varepsilon_{r1}} \csc \theta_1) \Psi_1 \quad \text{and} \quad d = a/\sqrt{\varepsilon_{r1}} \quad (3.4)$$

The ratio,  $\ell_2/\ell_1$ , is obtained from [2 (2.10)] as

$$\frac{\ell_2}{\ell_1} = \frac{-1 + \sqrt{\varepsilon_{r2}} (-\cot \theta_1 + \csc \theta_1)}{-1 - \cot \theta_1 + \sqrt{\varepsilon_{r2}} \csc \theta_1} \quad (3.5)$$

Next, the ratio,  $\Psi_2/\ell_1$ , is calculated from [2 (2.19)] as

$$\frac{\Psi_2}{\ell_1} = \frac{1 - \ell_2/\ell_1}{\cot \theta_1} \quad (3.6)$$

Finally, from Figure 4 on page 10, the thickness of the lens on axis is just,  $\ell_0 = \ell_1 - (a + d)$ . Thus, in terms of lens thickness, we can write

$$\Psi_2 = (\ell_0 + a + d) \frac{\Psi_2}{\ell_1} \quad (3.7)$$

The minimum allowable lens output radius,  $\Psi_{2,\min}$ , occurs for  $\ell_0 = 0$ .

Equation (3.7) can be used to determine the  $\Psi_2$  required to produce any desired lens thickness, or any value larger than  $\Psi_{2,\min}$  may be chosen, for example, to satisfy an electrical breakdown constraint. The design is completed by calculating  $\ell_1$  from the ratio produced by (3.6), and  $\ell_2$  from the ratio generated by (3.5).

#### 4. Sample Design Calculation for a HIRA with an Offset Feed and 0.40 $F/D$ Ratio

We apply the design approach just derived to the case of a  $100\ \Omega$  HIRA driven by a cylindrical transmission line with offset inner conductor. The impedance of the oil-filled transmission line is  $67\ \Omega$  ( $100\ \Omega$  in air). Thus,  $f_g = Z_C / Z_0 = 100/376.727$ . We postulate a peak driving voltage,  $V_0$ , of 2.6 MV, and a maximum permissible electric field in the transmission line,  $E_{\max}$ , of 2 MV/cm. Although we assume a single conical feed for the half reflector, in practice, this can be replaced by a pair of equivalent  $200\ \Omega$  feed cones, as depicted later in Figure 9 (on page 19). Table I summarizes the parameters that served as input to the calculation of the offset feed line design. Table II lists the resulting feed line dimensions.

The charge center output angle,  $\beta_0$ , the radius at the charge center in the input feed,  $\Psi_{CC1}$ , and the radius of the outer conductor,  $\Psi_1$ , are then used in a lens design calculation, as described above and in [2]. The lens design assumes that the transmission line is filled with oil having a relative dielectric constant of 2.2, while the lens is assumed to have a relative dielectric constant of 7.0. The maximum radius of the lens was set to 13 cm.

Table I. Parameters used to calculate the offset transmission line design.

Parameter	Value	Source
$f_d$	0.400000	Assumed
$Z_C$	100.000 $\Omega$	Assumed
$V_0$	2.6 MV	Assumed
$E_{\max}$	2 MV/cm	Assumed
$f_g$	0.265444	$Z_C/Z_0$
$\beta_0$	64.0108°	(2.1)
$\vartheta_0$	21.3671°	$90^\circ - \beta_0$
$\Psi_{CC1}/\Psi_1$	0.230769	(2.6)
$d/\Psi_1$	2.05128	(2.10)
$u_1$	1.46634	(2.14)
$u_0$	3.13417	(2.15)
$d/\Psi_0$	11.4630	(2.16)
$\Psi_0/\Psi_1$	0.178947	(2.17)
$\Psi_{CC0}/\Psi_1$	0.00779062	(2.18)
$\Psi_{1,\min}$	4.75229 cm	(2.23)

Table II. Offset transmission line dimensions.

Item	Parameter	Value	Source
Radius of outer conductor	$\Psi_1$	4.75 cm	Chosen $\geq \Psi_{1,\min}$
Radius of inner conductor	$\Psi_0$	0.849998 cm	$(\Psi_0/\Psi_1) \Psi_1$
Offset of axis of inner conductor from axis of outer conductor	$\Psi_B$	1.05915 cm	$(\Psi_{CC1}/\Psi_1 - \Psi_{CC0}/\Psi_1) \Psi_1$

Table III summarizes both specified and calculated lens design parameters. For the lens design, the ground plane is normal to the symmetry axis of the lens. The coordinate system origin,  $(z, \Psi) = (0,0)$ , is at the intersection of the symmetry axis and ground plane. With the exception of  $\Psi_{0,\text{lens}}$ , the parameter symbols used in the table are those detailed in [2] and identified on page 10 in the lens design sketch (Figure 4). In Figure 5, a sketch based on the parameters listed here is overlaid with the offset transmission line design results presented previously in Table II.

Table III. Lens design parameters for use with an offset transmission line feed for a  $F/D = 0.4$  HIRA.

Item	Parameter	Value	Source
<b>Specified Values</b>			
Coax dielectric constant	$\varepsilon_1$	2.20000	Assumed
Lens dielectric constant	$\varepsilon_2$	7.00000	Assumed
Output dielectric constant	$\varepsilon_3$	1.00000	Assumed
Output ray cone angle	$\vartheta_0$	25.9892°	90° - $\beta_0$
Charge center radius	$\Psi_{0,\text{lens}}$	1.09615 cm	$\Psi_{\text{CC1}}$
Outer conductor radius	$\Psi_1$	4.75000 cm	Offset choice
Lens radius at ground plane	$\Psi_2$	13.0000 cm	Assumed, (3.7)
<b>Calculated Values</b>			
Impedance constant	$K_Z$	4.33334	$\cot(\vartheta_0/2)$
Charge center flare angle	$\theta_0$	7.10°	(3.2)
Outer conductor flare angle	$\theta_1$	55.24°	(3.2)
Ellipsoid semi-major axis length	$a$	5.737 cm	(3.4)
Ellipsoid focal length	$d$	3.216 cm	(3.4)
Ellipsoid focal point to quartic surface distance	$\ell_1$	12.058 cm	$\Psi_2/(\Psi_2/\ell_1)$
Quartic surface location	$\ell_2$	3.036 cm	$(\ell_2/\ell_1)\ell_1$
Lens thickness on-axis	$\ell_0$	3.105 cm	$\ell_1 - d - a$
<b>Interface Intersections</b>			
Ellipsoid—charge center	$(z_0, \Psi_0)_{\text{lens}}$	(-0.224 cm, 1.096 cm)	Ray tracing
Outer feed conductor—lens	$(z_1, \Psi_1)$	(-5.725 cm, 4.750 cm)	Ray tracing
Quartic—charge center	$(z_3, \Psi_3)$	(3.097 cm, 1.510 cm)	Ray tracing

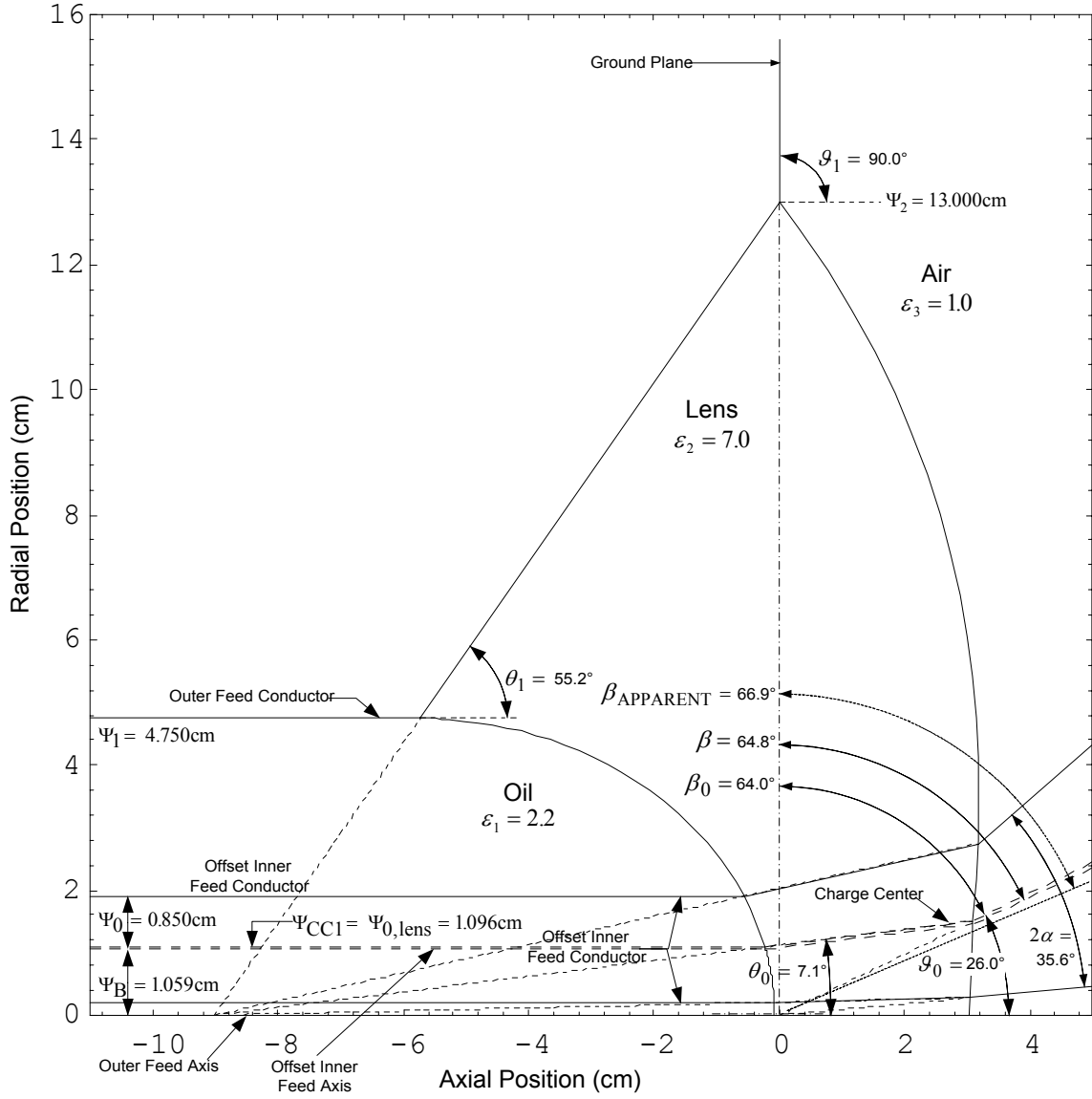


Figure 5. Offset transmission line with symmetric feed-point lens for a  $100 \Omega$  half reflector IRA with a  $0.40 F/D$  ratio.

An examination of the comparison of predicted and observed (based on ray tracing) feed cone parameters presented below in Table IV reveals that the design developed here is approximate, since only the charge center exit ray angle,  $\beta_0$ , agrees exactly with the theory. The apparent or ray cone-based output impedance is calculated by inversion of (2.3) as

$$Z_C = \frac{Z_0}{2\pi} \operatorname{arccosh} \left( \frac{\sin \beta}{\sin \alpha} \right) \quad (4.1)$$

where we interpret the observed ray cone angle as  $2\alpha$ , and the apparent axis of the ray cone,  $\beta_{\text{APPARENT}}$ , defines  $\beta$ . The impedance, implied by this exit envelope of the rays that define the extremes of the offset inner conductor, is  $105.83 \Omega$ , about 6% high.

Table IV. Comparison of predicted and observed feed cone parameters.

<b>Feed Cone Parameter</b>	<b>Predicted Value</b>	<b>Based on Ray Exit Angles from Lens</b>
$\beta_0$	$64.0108^\circ$	$64.0108^\circ$ (charge center ray)
$\beta$	$67.7335^\circ$	$64.7856^\circ$ (axial ray)
$\beta_{\text{APPARENT}}$	$67.7335^\circ$	$66.9400^\circ$ (ray envelope center line)
$2\alpha$	$39.4096^\circ$	$35.6392^\circ$ (ray envelope)
$Z_C$	$100.00 \Omega$	$105.83 \Omega$ ( $\alpha, \beta_{\text{APPARENT}}$ , (4.1))

## 5. Discussion of the Results of the Sample Offset HIRA Design Calculation

To explore the deviations between our predicted and “observed” ray tracing results (Table IV, above), we next consider the differing functional forms of the electrical potential within the feed-point lens system. Three regions may be identified: (1) the oil-filled coaxial input region, (2) the biconic lens region, and (3) the monocone-over-ground plane output region. For a plane wave propagating in the axial ( $z$ ) direction within the coaxial region, a ray initially at the radial coordinate,  $\Psi = \Psi_C$  (the coaxial insertion radius), where  $a < \Psi_C < b$  (Figure 6), follows an equipotential within each region. However, except at the surfaces of the conductors, the geometrically traced ray follows a different equipotential within each region.

We now develop expressions for the potential function in each region and calculate the extent of the shifts in potential identified above. First, in the input coaxial region, we need the potential as a function of the cylindrical radius,  $\Psi$ . The potential on the center conductor is  $V = V_0$ ; on the outer conductor, it is  $V = 0$ . Thus, between the conductors, the potential as a function of radius is given by

$$V(\Psi) = V_0 \frac{\ln(\Psi/b)}{\ln(a/b)} \quad (5.1)$$

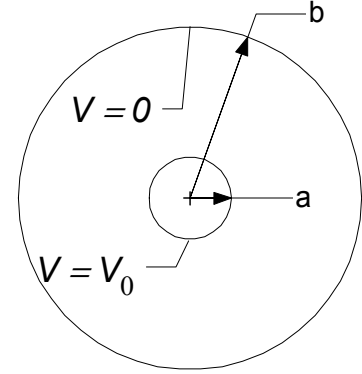


Figure 6. Coaxial geometry.

Next, for the biconic lens region, we implement a stereographic projection in the direction of the axis. The result is another coaxial geometry. In the following set of equations for the projection,

note that the parameter,  $R_0$ , is arbitrary.

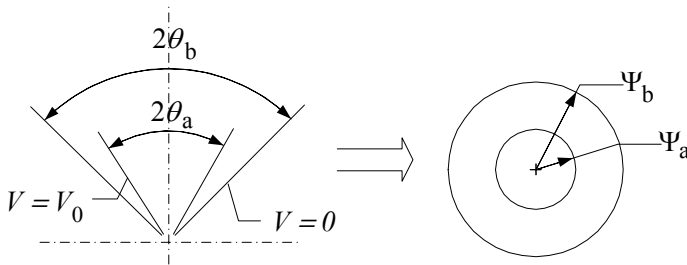


Figure 7. Stereographic projection of a pair of coaxial cones joined at the vertex leads to a coaxial cylindrical geometry.

$$\begin{aligned} \Psi &= 2R_0 \tan(\theta/2) \\ \Psi_a &= 2R_0 \tan(\theta_a/2) \\ \Psi_b &= 2R_0 \tan(\theta_b/2) \end{aligned} \quad (5.2)$$

Now, from (5.1) and (5.2), the potential of the projected structure is

$$V(\Psi) = V_0 \frac{\ln\left(\frac{\tan(\theta/2)}{\tan(\theta_b/2)}\right)}{\ln\left(\frac{\tan(\theta_a/2)}{\tan(\theta_b/2)}\right)} \quad (5.3)$$

This expression is applicable to the region interior to the lens, where the flare of the outer conductor forms the outer cone and the flare of the center conductor forms the inner cone. Outside the lens, the geometry is that of an upright monocone over a ground plane. Here,  $\theta_b \rightarrow 90^\circ$ ; and (5.3) reduces to

$$V(\Psi) = V_0 \frac{\ln(\tan(\theta/2))}{\ln(\tan(\theta_a/2))} \quad (5.4)$$

The normalized voltage functions,  $V(\Psi)/V_0$ , for input coaxial, lens biconic, and output monocone regions, as functions of the coaxial insertion radius,  $\Psi_C$ , were computed for the lens

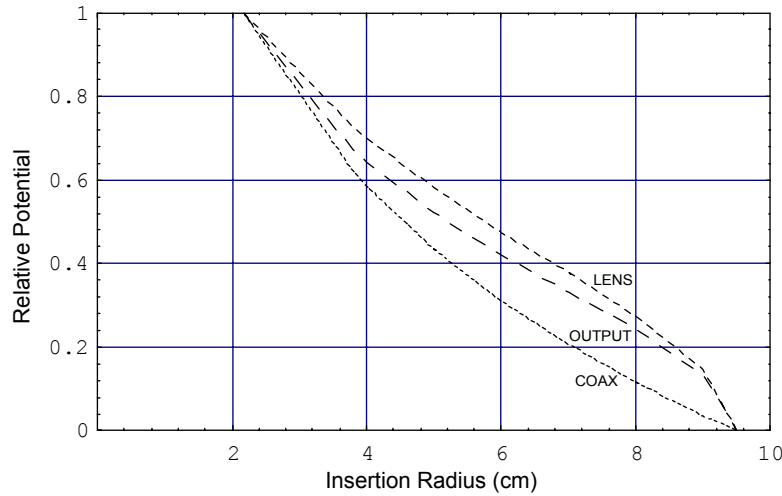


Figure 8. Relative potentials for a rotationally symmetric feed-point lens design. The potentials are shown within the input feed (coaxial region), within the lens (bicone region), and at the lens output (monocone region), as functions of the coaxial insertion radius.

designed in the preceding example. The results are presented in Figure 8. These results indicate that all rays, except those at the conductor surfaces, experience a different potential within each region. The magnitude of the potential shift at each interface is a function of insertion radius. The three curves in the figure give the relative potential as functions of the radial coordinate at insertion: for the coaxial insertion region, for the lens region, and for the lens output region. If our design theory were exact, these three curves would

overlap perfectly; and every inserted ray would remain on the *same* equipotential as it is ray-traced through the structure.

## 6. Offset HIRA Reflector Feed Considerations

Although our design calculations have assumed a single conical feed for the half reflector, in practice, this feed would be replaced by a pair of equivalent  $200\ \Omega$  feed cones, as depicted in Figure 9. Only the front view is shown here, as the side view is indistinguishable from that of the bent monocone shown in Figure 2 on page 4. This design has a disadvantage, however, in that the lens protrudes beyond the ground plane, and the feed arms should ideally be joined near the ground plane level, at the focus of the quartic surface of the lens.

This would require that the feed arms be joined inside the lens, a design that would be difficult to manufacture. If this situation were to become a problem, we could split the inner conductor before entering the lens, as shown below in Figure 10. Additionally, to minimize the impedance discontinuity, the transition from a single offset inner conductor to a pair of conductors could be made as gradual as might prove appropriate.

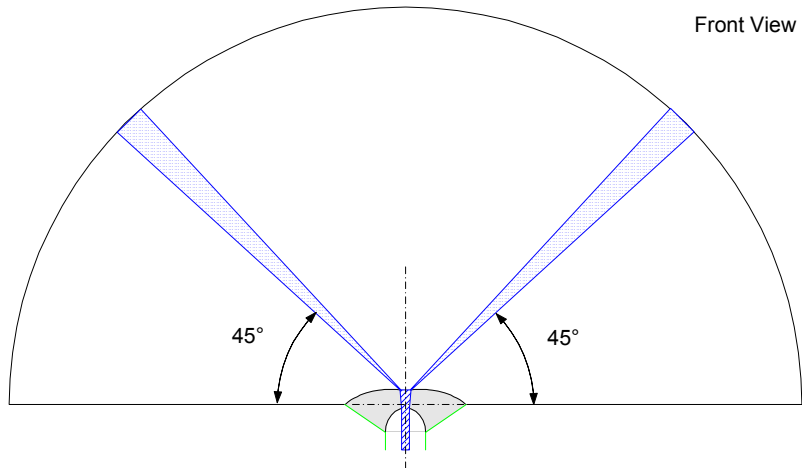


Figure 9. Offset HIRA fed by a pair of  $200\ \Omega$  cones. This feed cone arrangement has an impedance of approximately  $100\ \Omega$ .

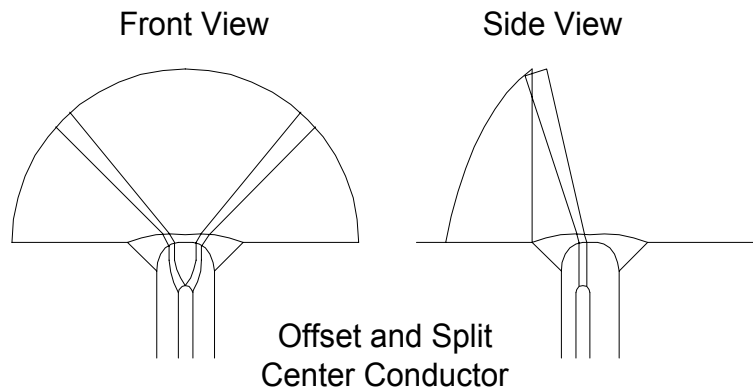


Figure 10. Offset and split inner conductor feed for a HIRA with  $F/D$  ratio larger than 0.25.

## 7. Concluding Remarks

We have provided a design approach for the feed-point lens and offset cylindrical feed line needed to build a high-voltage half IRA with an  $F/D$  ratio larger than 0.25. For the example with an  $F/D$  ratio of 0.40, the ray paths through the lens at the offset feed location are not quite correct. However, the impedance based on these rays is only slightly different from the design target. This difference may be related to the shifts in potential experienced by rays traversing the feed-point lens system. It seems unlikely that a significant impact on measurable HIRA performance can be expected to result from the approximate nature of this design approach.

## Acknowledgments

We would like to thank Mr. William D. Prather of Phillips Laboratory for funding this work. We would also like to thank Dr. Carl E. Baum for his many helpful discussions that contributed to this effort.

## References

1. E. G. Farr and C. E. Baum, Feed-Point Lenses for Half Reflector IRAs, Sensor and Simulation Note 385, November 1995.
2. W. S. Bigelow, E. G. Farr, and G. D. Sower, Design Optimization of Feed-Point Lenses for Half Reflector IRAs, Sensor and Simulation Note 400, August 1996.
3. E. G. Farr and C. E. Baum, Prepulse Associated with the TEM Feed of an Impulse Radiating Antenna, Sensor and Simulation Note 337, March 1992.
4. E. G. Farr, G. D. Sower, and C. J. Buchenauer, Design Considerations for Ultra-Wideband, High-Voltage Baluns, Sensor and Simulation Note 371, October 1994.
5. C. E. Baum, Impedances and Field distributions for Symmetrical Two Wire and Four Wire Transmission Line Simulators, Sensor and Simulation Note XXVII, 10 October 1966.
6. E. G. Farr, Optimizing the Feed Impedance of Impulse Radiating Antennas, Part I, Reflector IRAs, Sensor and Simulation Note 354, January 1993.
7. E. G. Farr and G. D. Sower, Design Principles of Half Impulse Radiating Antennas, Sensor and Simulation Note 390, December 1995.